Characterizing the Impact of In-Plane Deformation in Die-to-Wafer Hybrid Bonding from Die Warpage and Bonder Shape Effects

Chongyang Cai, Liu Jiang, El Mehdi Bazizi

Applied Materials Inc., Santa Clara, California, USA

Abstract

The increasing demand for high-performance computing and artificial intelligence is accelerating the adoption of advanced packaging technologies capable of supporting a higher number of interconnects with reduced pitch. Die-to-wafer (D2W) hybrid bonding has emerged as an important enabler for next-generation heterogeneous integration because it provides high-density interconnects with superior electrical performance. However, the process also introduces critical overlay challenges caused by mechanical deformation of the die during die chucking and bonding. In this work, a physics-based model is used to characterize in-plane deformation (IPD) in D2W hybrid bonding and to decouple the respective contributions from die chucking and bonding-induced deformation. The model captures the full bonding workflow, including incoming die warpage, vacuum chucking, bond-wave propagation, and final die-substrate gap closure. The results show that the final post-bonding IPD originates from two coupled sources: deformation introduced when the die is attached to the bonding head and additional deformation generated as the bonding wave propagates during hybrid bonding. Both contributions depend strongly on the incoming die warpage and on the bonder pedestal shape. For dies bonded with a symmetric round pedestal, the in-plane deformation remains nearly symmetric in the x and y directions. In contrast, strip-shaped pedestals introduce anisotropic deformation, and for a horizontal strip pedestal the in-plane deformation along the strip direction is shown to be largely dominated by post-chucking deformation, whereas the perpendicular direction contains a more significant bonding-induced contribution. The model results are consistent with measured die-stretching trends and provide a useful framework for optimizing incoming die warpage and bonder geometry to reduce overlay error in D2W hybrid bonding.

Keywords— die-to-wafer hybrid bonding, in-plane deformation, overlay, die stretching, die warpage, vacuum chucking, pedestal design

1. Introduction

Hybrid bonding has become one of the most promising integration schemes for advanced packaging because it enables very fine-pitch vertical interconnects with excellent electrical and mechanical performance. Compared with conventional assembly methods, hybrid bonding offers much higher interconnect density and is increasingly being adopted for memory stacking, chiplet integration, and heterogeneous system assembly[1]. In D2W hybrid bonding, plasma activation is used to prepare the bonding surfaces, after which low-temperature bonding and subsequent annealing establish dielectric bonding and Cu–Cu interconnection between the die and wafer.

Although D2W bonding provides important advantages over wafer-to-wafer integration, especially for heterogeneous integration and known-good-die assembly, it also introduces unique process sensitivities related to individual die handling. One of the critical issues is post-bond in-plane deformation, often captured experimentally as overlay (OVL) error or die stretching. This deformation directly affects copper-to-copper alignment and therefore becomes increasingly important as bonding pitch continues to shrink[2]. During bonding, the die first deforms when it is vacuum-attached to the bonder head, and it then undergoes further shape evolution as the bonding front propagates across the die. The center region of the die experiences tensile stress early in the bonding sequence because adhesion pulls the die downward while the outer region remains constrained by the bond head. Once this stretched region bonds to the substrate, the deformation becomes locked in, producing permanent post-bonding in-plane distortion. While this mechanism has been established and previously validated against measured die-stretching trends, the final post-bonding deformation observed after bonding still represents the combined effect of multiple process steps, making it difficult to determine how much of the final IPD originates from die chucking and how much is generated during bonding itself[3].

From a manufacturing perspective, reducing overlay error requires a process-level optimization strategy, since the final in-plane deformation is influenced by multiple coupled factors across the die handling and bonding sequence. Effective improvement therefore depends on understanding how incoming die condition, chucking behavior, bonding dynamics, and bonder design collectively contribute to the final deformation state[4]. A modeling framework that can decouple the chucking-

induced and bonding-induced components of IPD is needed to provide actionable guidance for tool design, recipe development, and incoming die specification.

Earlier work in Ref [3] established the core modeling framework for die, substrate, bonder interaction, interfacial adhesion, air resistance. The present work further extends the study by adding a standalone chucking simulation to quantify the in-plane deformation generated before wafer contact and compares that state with the final post-bonding deformation. The study also evaluates how bonder shape affects deformation symmetry, anisotropy, and the directional partitioning of chucking-induced and bonding-induced IPD. The post-chucking deformation contours, pedestal-comparison results, directional decoupling analysis, and corresponding discussion are evaluated to this manuscript.

To separate the origin of the final in-plane deformation in D2W hybrid bonding, a standalone chucking model is developed to quantify the post-chucking IPD independently from the complete bonding process, enabling direct comparison with the final post-bonding deformation. In parallel, different bonder configurations, including symmetric round pedestals and directional strip pedestals, are evaluated to understand how bonder geometry influences the magnitude, symmetry, and directional distribution of IPD. While a round pedestal tends to produce a more symmetric deformation field, strip-based designs introduce anisotropic constraint during chucking and bonding, which can amplify or isolate deformation in specific directions. These design-dependent effects are highly relevant to manufacturing, because they determine whether overlay error is primarily controlled by incoming die warpage, vacuum chucking conditions, or bonding-front propagation. By linking die deformation to bonder geometry and process sequence, this study provides practical guidance for optimizing bond-head design, pedestal layout, and chucking strategy in order to reduce overlay error and improve bonding robustness in high-density hybrid bonding applications.

2. Modeling Approach

The die-to-wafer hybrid bonding process considered in this study consists of a series of sequential steps: die attach, touchdown, vacuum release, and nozzle removal, as illustrated in Fig. 1. In the first step, the incoming die is picked up and held by the bonder nozzle through vacuum chucking. During this die-attach step, the die deforms to conform to the chucking surface, and an initial in-plane deformation is introduced before the die contacts the wafer. This deformation is referred to as the post-chucking IPD. After the die is aligned and brought into contact with the substrate, the bonding process begins at the initial touchdown location. As the bonding wave front propagates and the die-to-wafer gap closes, additional deformation develops due to the combined effects of surface interaction, die elasticity, and vacuum release. After the vacuum is removed and the nozzle retracts, the bonded die retains a final deformation state, referred to as the post-bonding IPD.

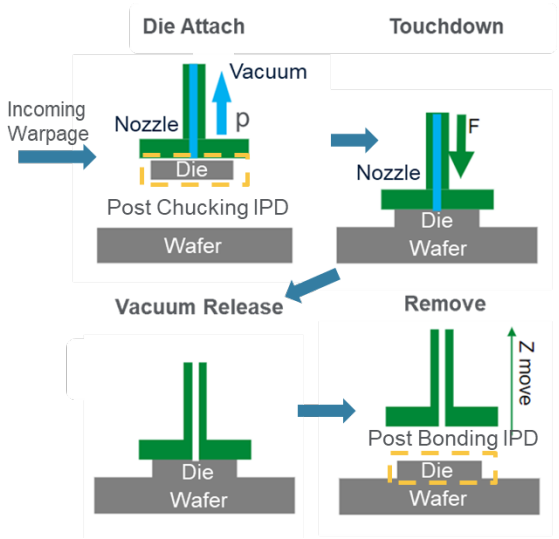


Fig. 1. Schematic of the D2W bonding process with post chucking IPD and post bonding IPD

The distinction between these two deformation states is important. The post-chucking IPD originates purely from the mechanical deformation caused by vacuum attachment of the warped die to the bonding head, whereas the post-bonding IPD includes both the chucking-induced contribution and the additional deformation accumulated during bond-wave propagation and final bonding. Therefore, the final overlay measured after bonding cannot be attributed to the bonding process alone but instead reflects the cumulative effect of both the chucking step and the subsequent bonding dynamics.

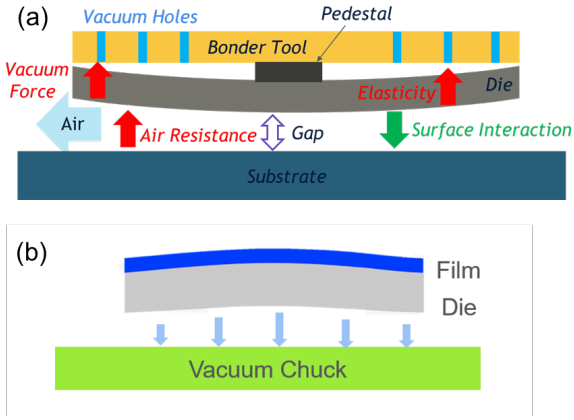


Fig. 2. Physics-based modeling framework for die-to-wafer hybrid bonding: (a) model including full bonding process (b) standalone chucking model for isolating post-chucking IPD.

To capture these coupled deformation mechanisms, a physics-based simulation platform is employed, as shown in Fig. 2(a). The model includes the bonder tool, the pedestal geometry, the incoming die with initial warpage, and the substrate. During bonding, the die is subjected to several competing forces. The adhesion or surface interaction between the die and the substrate drives die attachment and bond-front propagation. Opposing this motion are the vacuum holding force from the bonder, the mechanical resistance associated with die elasticity, and the air resistance trapped in the die-to-substrate gap. Interfacial adhesion is modelled using a modified 3–9 Lennard-Jones potential, capturing the dependence on local gap distance. Air resistance is incorporated through a CFD-based approach, which predicts the air resistance force versus die-substrate gap with a simplified Navier-Stokes equation for incompressible flow. These interactions collectively determine the transient shape evolution of the die and the final in-plane deformation after bonding. Initial die warpage is introduced through a stress-induced oxide layer to achieve convex or concave die shapes.

In order to decouple the contribution of die chucking from the total post-bonding deformation, a separate simulation is constructed to isolate the chucking process itself. As shown in Fig. 2(b), this standalone chucking model considers a warped die being vacuum-attached to a flat chucking surface, without including the subsequent bonding interaction with the wafer. In this case, the purpose of the simulation is to quantify only the deformation introduced when the die is pulled against the chuck by vacuum force.

This separate chucking model provides a direct measure of the post-chucking IPD, independent of bond-wave propagation and substrate interaction. By comparing the deformation predicted by the standalone chucking model with the final deformation obtained from the full bonding model, the relative contributions from chucking and bonding can be distinguished.

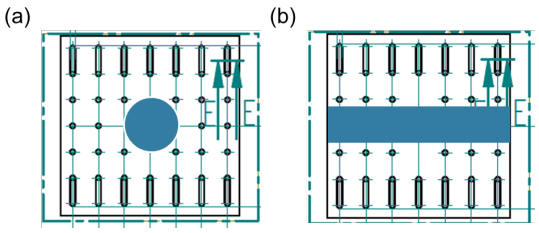


Fig. 3. Bonder design schematics: (a) round pedestal (b) strip pedestal

Two pedestal geometries are considered in the present modeling framework, as shown in Fig. 3: a round pedestal and a strip pedestal. The round pedestal represents a symmetric bonding-head design and is used as the reference case for evaluating deformation under nearly isotropic chucking and bonding conditions. Because the geometry is symmetric in the x and y directions, the resulting deformation pattern is expected to be similar in both directions unless asymmetry is introduced by the incoming die warpage.

In contrast, the strip pedestal introduces a strong directional preference into the process. Depending on the strip orientation, the die experiences different levels of support and constraint in the two in-plane directions. This anisotropic boundary condition alters both the chucking response and the bond-wave evolution, making the strip pedestal particularly useful for studying directional differences in IPD.

Besides from the pedestal shape effect, the die warpage is introduced through the film/die stack prior to bonding, resulting in either a convex or concave die profile depending on the stress condition. The warpage magnitude determines how much out-of-plane deformation must be corrected during chucking, while the warpage direction influences how the die first approaches the substrate and how the bond front propagates afterward. Both warpage magnitude and warpage direction are systematically considered in this study to understand their impact on the final deformation state.

3. Results and Discussion

3.1 Effect of Incoming Warpage on Bonding Gap Evolution and Post-Bonding IPD

The effect of incoming die warpage on the bonding process is first examined through the simulated bonding gap evolution, as shown in Fig. 4, for the concave 8 μm (+8 μm) and convex 33 μm (−33 μm) cases. The experimental dataset included 100 dies bonded using the round-pedestal design. In the concave 8 μm case, the gap evolution becomes highly non-uniform during propagation. After the initial center contact, the bonded region expands while rest edge peripheral areas are also getting closer to the wafer substrate due to the initial warpage shape, and the final gap shape shows corner-localized residual regions, indicating a bonding wave merging gap closure behavior, which may bring certain voiding formation risks. In contrast, the convex 33 μm case exhibits a much more symmetric and continuous

center-outward bond-wave propagation, with the bonded region expanding in a nearly circular manner throughout the process. These results confirm that the incoming die warpage not only affects the magnitude of deformation, but also significantly changes the bonding path and gap-closure pattern.

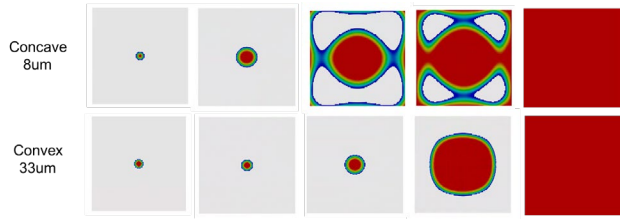


Fig. 4. Bonding-gap evolution for dies with different incoming warpages on round pedestal

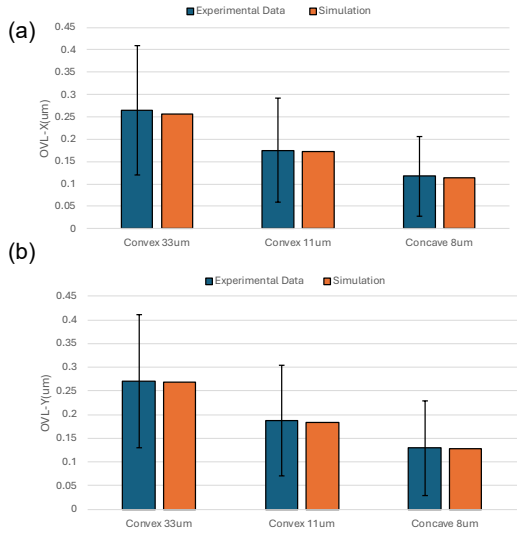


Fig. 5. Experimental and simulated post-bonding overlay comparison for different incoming warpage conditions

Post-bonding IPD was evaluated for three incoming die warpage conditions with convex 33 µm, convex 11 µm, and concave 8 µm, in order to assess the effect of warpage magnitude on the final deformation state. As shown in Fig. 5, both the experimental data and the simulation results exhibit a consistent trend in which the post-bonding overlay increases with increasing warpage magnitude. The convex 33 µm case produces the largest OVL-X and OVL-Y, the convex 11 µm case shows an intermediate level of deformation, and the concave 8 µm case yields the smallest post-bonding IPD. This trend indicates that the incoming die warpage magnitude is a dominant parameter controlling the extent of deformation retained after bonding. The close agreement between simulation and experiment across all three cases further confirms that the model is able to accurately capture the dependence of post-bonding IPD on the incoming warpage magnitude. The variation between experiment and simulation is within 15%.

3.2 Decoupling of Post-Chucking and Post-Bonding IPD for Round Pedestal

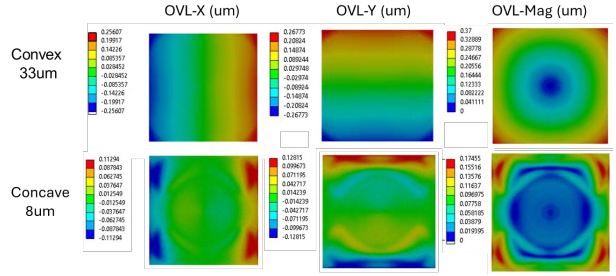


Fig. 6. Post-bonding IPD contour for dies with different incoming warpages on round pedestal

Fig. 6 shows the post bonding overlay for different incoming die warpages on round pedestal. The simulated post-bonding IPD contours clearly show that the overall deformation pattern remains highly symmetric, consistent with the laterally symmetric pedestal geometry. Comparing the two warpage cases, the die with larger incoming warpage exhibits a visibly stronger deformation response, as reflected by the broader spatial gradient in both OVL-X and OVL-Y and the larger high-displacement region in the OVL magnitude map. In both cases, the OVL-X and OVL-Y contours show similar deformation amplitudes and nearly mirror each other in orthogonal directions, indicating that the round pedestal does not introduce significant directional bias into the in-plane deformation. Correspondingly, the OVL magnitude distribution displays a concentric and symmetric pattern centered around the die middle, further confirming that the deformation evolves in an isotropic manner under the round pedestal design. These results indicate that, for a symmetric pedestal, the primary effect of increasing incoming warpage is to increase the overall IPD magnitude, while the deformation pattern itself remains balanced between the x and y directions.

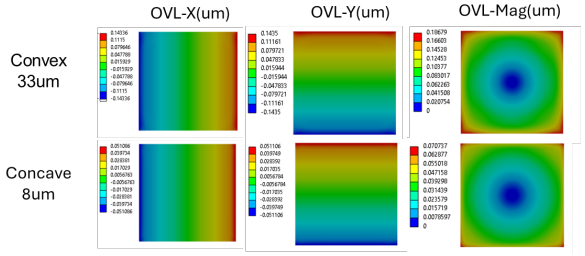


Fig. 7. Post-chucking IPD contour for dies with different incoming warpages on round pedestal

The post-chucking IPD contours is shown on Fig .7. For the round pedestal configuration, it shows that the deformation introduced during die chucking is already significant and follows a highly symmetric pattern. For both the convex 33 µm and concave 8 µm cases, the OVL-X and OVL-Y maps exhibit nearly identical spatial distributions in orthogonal directions, indicating that the chucking-induced deformation is well balanced between the x and y axes. This behavior is consistent with the laterally symmetric round pedestal and uniform vacuum loading, which do not impose a preferred in-plane direction during die attachment. As a result, the deformation field generated during chucking remains largely isotropic.

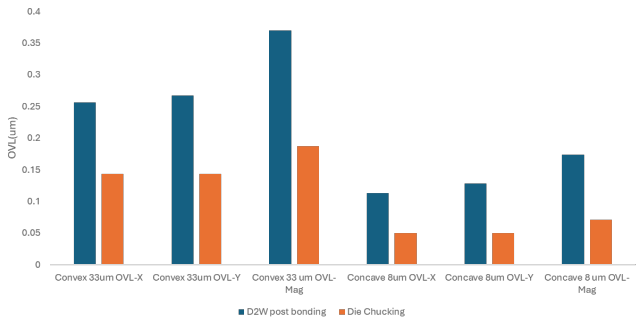


Fig. 8. Comparison of post-chucking IPD and post-bonding IPD for dies with different incoming warpages

A direct comparison between post-chucking and post-bonding IPD is listed in Fig. 8, which shows that the deformation introduced during die chucking already accounts for a substantial fraction of the final post-bonding deformation. For both the convex 33 µm and concave 8 µm cases, the post-chucking IPD is approximately half of the corresponding post-bonding IPD, indicating that the final overlay is not generated by bonding alone, but rather results from the cumulative contributions of die chucking and subsequent bond-wave propagation.

3.3. Horizontal Strip Pedestal: Directional Decoupling of Post-Chucking and Post-Bonding IPD

The horizontal strip pedestal introduces a strongly anisotropic bonding condition compared with the round pedestal case. As shown by the bonding-gap evolution sequence in Fig. 9, the initial contact is not point-like or circular, but instead forms an elongated bonded region aligned with the strip direction. As bonding proceeds, the bonded area expands mainly in the direction perpendicular to the strip, while remaining extended along the strip axis throughout the process. This behavior indicates that the strip pedestal imposes a directional constraint during bonding and therefore changes both the bond-wave propagation path and the way deformation is accumulated in the die. Unlike the round pedestal, which promotes a nearly isotropic center-outward bonding pattern, the strip pedestal produces a bonding front that is inherently direction-dependent.

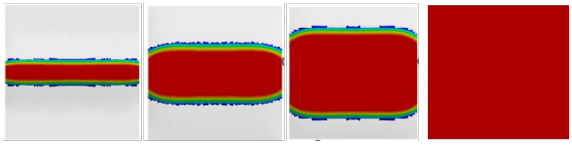


Fig. 9 Bonding-gap evolution for dies with concave 8 µm warpages on strip pedestal

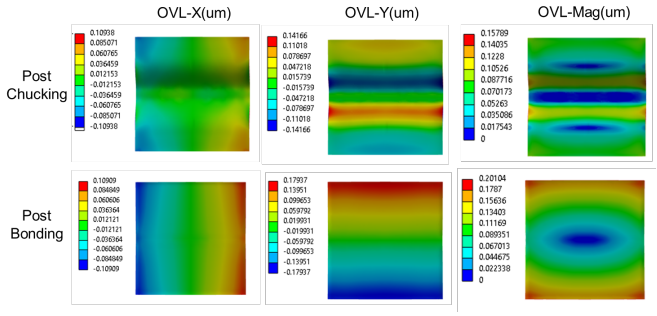


Fig. 10 IPD contour comparison of post chucking and post bonding for dies with concave 8µm incoming warpage on strip pedestal

The corresponding post-chucking and post-bonding IPD contour maps further show this directional effect. As shown in Fig. 10, in the post-chucking condition, the deformation field is already anisotropic, with the largest displacement concentrated around the region influenced by the strip-shaped chucking contact. The OVL-X, OVL-Y, and OVL magnitude maps all show that the strip geometry introduces a non-uniform deformation pattern that is no longer symmetric in all in-plane directions. After the full bonding process, the deformation field becomes smoother and more global, but the directional difference remains evident. In particular, the post-bonding OVL-X maximum values remains similar to the post-chucking result, indicating that the deformation along the strip direction is primarily established during the chucking step. In contrast, the post-bonding OVL-Y map shows a clearer increase in deformation compared with the post-chucking state, indicating that additional IPD is generated during bond-wave propagation and final gap closure in the direction perpendicular to the strip.

The OVL magnitude maps provide the clearest overall view of this decoupling behavior. For the post-chucking condition, the magnitude distribution is more localized and closely tied to the strip-contact region, whereas after

bonding the magnitude becomes larger and more broadly distributed across the die. However, the spatial pattern still reflects the directional nature of the strip pedestal. These results indicate that, for the horizontal strip pedestal, the deformation along the strip direction is largely chucking-dominated, while the deformation in the perpendicular direction contains a stronger bonding-induced contribution. This makes the strip pedestal useful for separating the origin of the final IPD and for identifying how bonder geometry influences the directional partitioning of overlay error.

4. Conclusion

In this work, a physics-based modeling framework was developed to decouple the origin of in-plane deformation in D2W hybrid bonding. By combining a full bonding simulation with a standalone chucking model, the results show that the final post-bonding IPD is the cumulative result of die chucking and bond-wave propagation rather than a purely bonding-generated effect. Incoming die warpage was found to strongly affect both bonding gap evolution and final IPD, and the simulated post-bonding deformation correlated well with experimental data for convex and concave warpage conditions. For the round pedestal, the deformation remained largely symmetric in x and y, while the post-chucking IPD accounted for approximately half of the final post-bonding IPD. For the horizontal strip pedestal, the deformation became anisotropic, with the strip direction dominated by chucking-induced deformation and the perpendicular direction showing a stronger bonding-induced contribution. These results demonstrate that both incoming die condition and bonder design play critical roles in controlling overlay error, and that the proposed modeling framework provides useful guidance for process optimization and bonder design in advanced hybrid bonding.

References

[1] C.-K. Hsiung and K.-N. Chen, “A Review on Hybrid Bonding Interconnection and Its Characterization,” IEEE Nanotechnology Magazine, vol. 18, no. 2, pp. 41–50, Apr. 2024, doi: 10.1109/MNANO.2024.3358714.

[2] G. Mehta, J. Abdilla, R. Hung, E. Bazizi, Y. C. Bum, D. Bikajlevic, L. Jiang, and G. Costrini, “D2W Hybrid Bonding Challenges for HBM,” in 2024 IEEE International Memory Workshop (IMW), 2024, pp. 1–4, doi: 10.1109/IMW59701.2024.10536945.

[3] Y. Lu, B. Pressl, K. Zheng, L. Jiang, Y. W. Wang, H. Kostner, C. Scanlan, R. Hung, and E. Bazizi, “Investigation of Post-Bonding Die Stretching in Die-to-Wafer Hybrid Bonding,” 2025 Symposium on VLSI Technology and Circuits, Paper T21-2, 2025.

[4] B. S. S. C. Rao, M. D. Kumar, V. N. Sekhar, I. C. Daniel, S. K. Tippabhotla, S. C. Chong, H. K. C., and V. S. Rao, “Dielectric Stack Optimization for Die-level Warpage Reduction for Chip-to-Wafer Hybrid Bonding,” in 2024 IEEE 74th Electronic Components and Technology Conference (ECTC), 2024, pp. 62–68, doi: 10.1109/ECTC51529.2024.00019.